J Appl Electrochem (2012) 42:47–57
DOI 10.1007/s10800-011-0370-4

ORIGINAL PAPER

Investigations on thiourea content in ternary Sn–Ag–Cu bath using electrochemical studies

Shany Joseph · Girish J. Phatak

Received: 17 April 2010 / Accepted: 3 March 2011 / Published online: 2 December 2011

Abstract We have developed a methane sulfonic acid (MSA) based ternary electrolytic bath for co-deposition of the eutectic Sn–Ag–Cu films. The bath contains thiourea (TU), which functioned as an effective chelating agent in controlling the bath stability as well as the elemental and microstructural properties of the deposited film. A study of the bath behaviour at TU concentrations in the range 0.06–0.2 M is undertaken with the help of elemental and microstructure analysis, cyclic voltammetry (CV) and impedance analysis. The deposited films have close to eutectic composition with slightly higher Cu content for all the TU concentrations. On the other hand, the microstructure is found to be increasingly refined with increasing TU content. The CV and impedance analysis confirm chelation of Ag and Cu with TU and absence of such chelation with Sn ions. It also indicates close deposition potentials for each metal ion. Impedance analysis specifically reveals presence of an adsorbed insulating film on cathode surface, contributed by MSA or water. It also reveals competitive deposition between the insulating film and metal ions.

Keywords Ternary Sn–Ag–Cu bath · Lead free solders · Thiourea · Impedance analysis · Cyclic voltammetry

S. Joseph · G. J. Phatak (✉)
Electronic Packaging Group, Centre for Materials for Electronic Technology (C-MET), Panchwati, Off Pashan Road, Pune 411 008, India
e-mail: gjp@cmet.gov.in

1 Introduction

Electrodeposition of solders is a common need in electronics and various industrial applications. Recently, Sn–Ag–Cu is seen as a potential 'lead-free' replacement of the Sn–Pb solders [1–5]. Due to the focus on micro-scale features in electronics, such as solder bumps, electrodeposition is seen as most useful process for obtaining lead-free solder films. Realizing such applications requires good control over the process. Any deviation in composition or dimensions would question its reliability and render it useless for the critical applications. Surely, it is essential to have a stable electrodeposition bath which is consistent over a wide range of process parameters.

The electrodeposition of Sn–Ag–Cu films can be done either sequentially using individual metal baths or simultaneously using ternary co-deposition bath. Development of co-deposition plating bath is a difficult task due to complexities introduced by the multi-component electrolyte, such as large difference in deposition potentials, mutual compatibility issues of bath components, etc. However, once optimized, the single step co-deposition process would have advantages over the multi-step sequential deposition process in terms of repeatability and composition control at microscopic level.

We have developed a ternary electroplating bath for co-deposition of eutectic Sn–Ag–Cu films with 95.7Sn–3.5Ag–0.8Cu compositions [6]. This bath is based upon methane sulfonic acid (MSA), uses thiourea (TU) as chelating agent and other additives as surfactant and surface finishing agent. It has been shown earlier that the MSA based ternary Sn–Ag–Cu deposition baths produce good quality solder films when used with additives, such as, Tris-3-hydroxypropyl phosphine (T3HPP), polyoxyethylene-α-naphthol (POEN) and 2,2′-dithiodianiline (DTDA).

An appropriate combination of the three additives helped in inhibiting preferential deposition of Cu^{2+} and Ag^{+} ions and produced a fine semi-lustrous Sn–Ag–Cu alloy film [7].

Electroplating of ternary metal system is an intricate process that needs thorough understanding of the microscopic processes happening in the vicinity of the electrode surface and in the electrolytic bath. This requires detailed investigations about the complex coordination between the chelating agents, surfactants and various other additives with the multiple metal ions. Amongst these, the chelating agents that allow co-deposition and ensure bath stability are the most important compounds. TU is one such known chelating agent. It is known that TU coordinates with both copper and silver [8] but the stability constant of thiourea-copper chelate is slightly more that of thiourea-silver, causing preferred chelation with copper [9]. Further, the stability of a particular complex would also be affected by the presence of the second metal ion and the pH of the solution. The competitive chelate formation would have an effect on the reaction mechanism and hence the deposited film composition. Such microscopic issues can be understood with the help of cyclic voltammetry (CV) and the frequency dependent impedance analysis of the plating baths.

The nature of the Nyquist plots derived from the impedance analysis helps in assigning these components to the microscopic processes. There are reports of impedance analysis of individual and binary Sn–Ag or Sn–Cu [10, 11] systems, but such study for the ternary baths of these elements is not reported yet. We have carried out the impedance analysis and CV of our Sn–Ag–Cu co-deposition bath in order to understand the deposition process in such baths. Particularly, this work is aimed at studying the effect of TU concentration on the deposited Sn–Ag–Cu film quality and composition with the help of impedance studies of the ternary electrolyte. The impedance spectra are analyzed and interpreted to understand the microscopic mechanisms during deposition and their effect on the physical properties of the deposited film.

2 Experimental

The ternary plating bath reported here is based on MSA and contains sulphate salts of copper and silver, and the methane sulphonate salt of tin. TU is used as a chelating agent and iso-octyl phenoxy polyethoxy ethanol (OPPE) is used as a surfactant. Gelatin served as a surface finishing agent. We have previously reported that TU holds only silver and copper ions in chelation and there is a positive contribution from OPPE in improving bath stability, mostly through hydrogen bonding with the constituent metal ions. It is also suggested that Sn ions may also be entering into some kind of loose bonding with the additives present in the bath [6]. This bath is now subjected to further detailed investigations to find the effect of TU on film properties and to understand the deposition mechanism at microscopic level. For the present studies, the concentration of TU was varied from 0.06 to 0.2 M while keeping all the other constituents and their concentrations constant. These baths are labeled as TU1 to TU4 in the increasing order of TU concentration. The details of the bath constituents used here are given in Table 1.

All the electrodepositions reported here were carried out at room temperature for 1 h and at a current density of 10 mA cm^{-2} (36 C·cm^{-2}). Ni plated Cu clad substrates with a pre-defined area of about 1 cm^2 were used as cathode, while pure Sn rod served as anode. A potentio-galvanostat (Autolab PGSTAT 100 with GPES® module) in the galvanostatic mode was used for carrying out these depositions. The microstructure and elemental composition of the electrodeposited films were studied using scanning electron microscope and energy dispersive X-ray spectrometer (SEM-EDS, Philips XL-30 with EDAX®). Separate electrochemical investigations on the ternary baths were carried out through the studies of CV and impedance analyses in the frequency range of 1 MHz to 1 mHz. The impedance analyses were carried out with the help of frequency response analysis (FRA) mode of potentio-galvanostat. All the electrochemical analyses were done under

Table 1 Plating bath composition for Sn–Ag–Cu Alloys

Bath constituents	TU0[a]	TU1	TU2	TU3	TU4
MSA (g L^{-1})	100	100	100	100	100
Tin methane sulfonate (g L^{-1})	140	140	140	140	140
Silver sulphate (g L^{-1})	0.1	0.1	0.1	0.1	0.1
Copper sulphate (g L^{-1})	0.02	0.02	0.02	0.02	0.02
TU (M)	0	0.06	0.13	0.16	0.26
OPPE (g L^{-1})	12	12	12	12	12
Gelatin (g L^{-1})	2	2	2	2	2
pH	~4				
Deposition temperature	Room temperature				

[a] This composition was used only for individual metal bath systems

static conditions using a 3 mm diameter bare platinum disc as the cathode and a glassy carbon electrode as the anode. A standard calomel electrode served as reference electrode. Additional CV curves for TU4 bath were also recorded at varying scan speed in order to judge the reversibility and to verify presence of diffusion control, if any. During the course of studies it was found prudent to investigate the individual ion baths using identical methods. Thus, separate baths for Sn, Cu and Ag ions were prepared with identical concentrations and other constituents. The CV and impedance analyses of these baths were also carried out under identical conditions. Due to the absence of stability issues in individual ion baths, an additional bath with zero TU content (TU0) could be prepared and subjected to similar analysis. The results are discussed below.

3 Results and discussion

3.1 Microstructure and composition

The Sn–Ag–Cu films deposited at 10 mA cm^{-2} (36 C·cm^{-2}) current density were characterized for their microstructure and elemental composition. Figure 1 presents surface morphology of these films deposited using baths having different TU content. It is seen that all the films have compact microstructure and exhibit adequate cathode coverage. All the films reveal fine crystalline microstructure with an average particle size of about 3–5 μm. It is observed that the granule size in the films becomes finer and the films become smoother with increasing TU content. The intermittently observed pores on the film surface also reduce with increasing TU content. These results confirm the contribution of TU in improving and refining the microstructure. TU in the electrolytic bath is known to perform multiple functions. Apart from chelating Ag and Cu [6], it also acts as brightener and leveling agent [12, 13].

The elemental composition of all the films is in desired range, although the Cu content is relatively large and varies between 1.4 and 3.9%. Figure 2 presents the dependence of the elemental composition of the films on the TU content in the baths. It is seen that the change in TU does not have any significant effect on the film composition. It may be noted that the entire range of TU content in these baths is more than adequate to chelate all the Ag^{+} and Cu^{2+} ions present [8], possibly making the elemental composition independent of TU content. The reactions of silver and copper with TU can be written as [8, 12]:

$$Ag^{+} + TU \rightarrow Ag(TU)^{+} \quad (1)$$

$$Ag^{+} + 2TU \rightarrow Ag(TU)_{2}^{+} \quad (2)$$

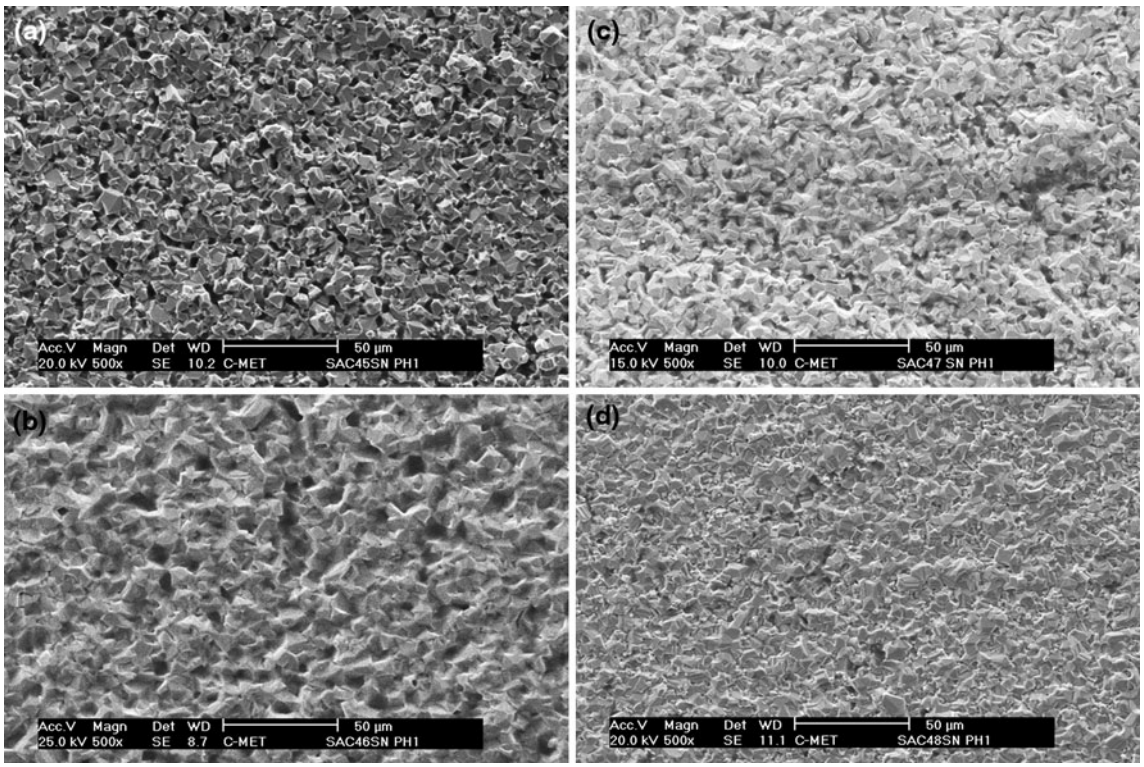

Fig. 1 SEM microstructure of ternary films deposited at room temperature for 1 h and 10 mA cm^{-2} current density (36 C·cm^{-2}) using bath compositions **a** TU1, **b** TU2, **c** TU3, and **d** TU4 (Table 1)

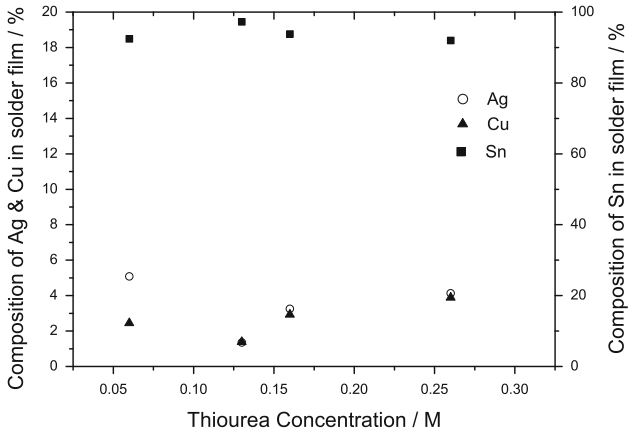

Fig. 2 Effect of TU concentration on the elemental composition of electrodeposited Sn–Ag–Cu films deposited at room temperature for 1 h and 10 mA cm^{-2} current density (36 $C{\cdot}cm^{-2}$)

$$Ag^{+} + 3TU \rightarrow Ag(TU)_3{}^{+} \quad (3)$$

$$Cu^{2+} + 2TU \rightarrow Cu(TU)^{+} + \frac{1}{2}FDS^{2+} \quad (4)$$

$$Cu^{2+} + 3TU \rightarrow Cu(TU)_2{}^{+} + \frac{1}{2}FDS^{2+} \quad (5)$$

$$Cu^{2+} + 4TU \rightarrow Cu(TU)_3{}^{+} + \frac{1}{2}FDS^{2+} \quad (6)$$

$$Cu^{2+} + 5TU \rightarrow Cu(TU)_4{}^{+} + \frac{1}{2}FDS^{2+} \quad (7)$$

Here, FDS is formamidine disulfide, which is represented as:

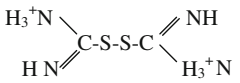

Simultaneously, the oxidation of TU also leads to the formation of FDS:

$$2TU \leftrightarrow FDS + 2e^{-} + 2H^{+} \quad (8)$$

In the given pH range and the concentrations of metal ions and TU, it is expected that only $(CuTU)_4^+$ and $(AgTU)_3^+$ chelates would be existing. It may be noticed that in the presence of TU, Cu^{2+} gets reduced to Cu^{+} and forms various complexes [14].

3.2 CV studies

The ternary solder deposition baths were studied with the help of CV. The cyclic voltammetric curves of this series of bath are presented in Fig. 3. It is seen from this figure that the CV curves for all the baths show a broad reduction peak, which signifies effective chelation of metal ions and points towards co-deposition in a narrow range of

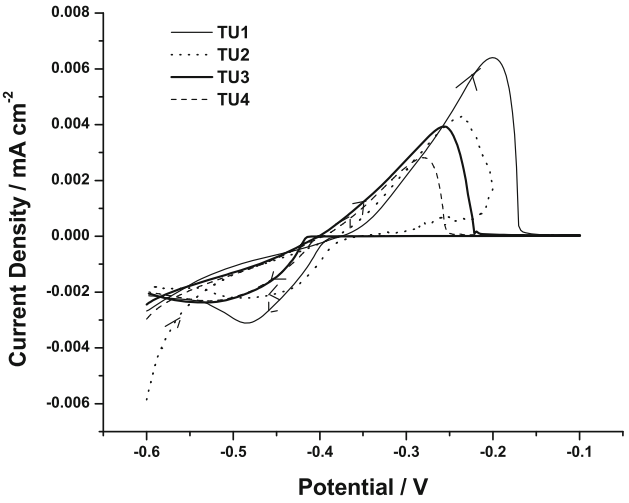

Fig. 3 Cyclic voltammetric curves of ternary baths with compositions TU1–TU4 (Table 1)

potentials. The apparent difference in peak oxidation and reduction currents is largely due to the baseline shift. Continuous broadening of the reduction peak with increasing TU content can be noticed. Possibly, the different complexes in the bath are reducing at close potentials. The broadening makes it difficult to identify exact peak position, although the total range is small, within 16 mV. It is also observed that there is continuous reduction in the peak current for both oxidation and reduction peaks. This indicates possibility of increased adsorption of an inhibiting compound on the cathode surface reducing the effective cathode area.

The reversibility of the process was verified by recording CV curves at different scan rates. Figure 4 presents the CV curves for the TU4 bath at different scan rates and the dependence of peak cathodic current I_{pc} on the square root

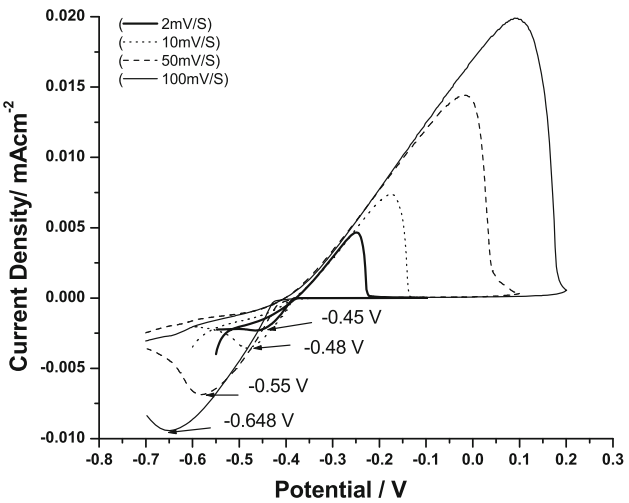

Fig. 4 Cyclic voltammetric curves of ternary baths with composition TU4 (Table 1) at varying scan rates

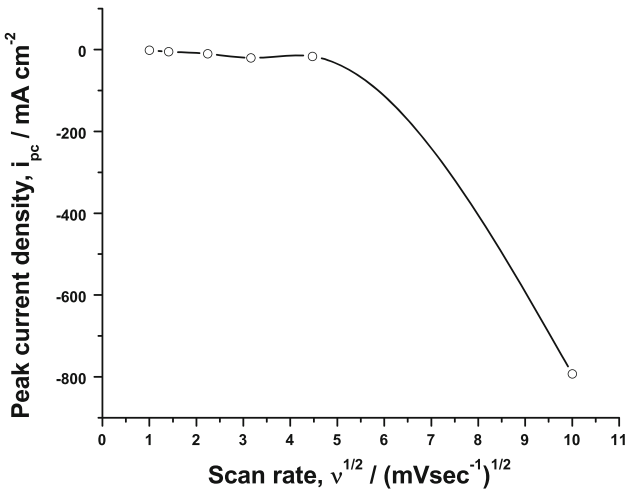

Fig. 5 The dependence of peak cathodic current I_{pc} on the square root of scan rate ($v^{1/2}$) for bath TU4 (Table 1)

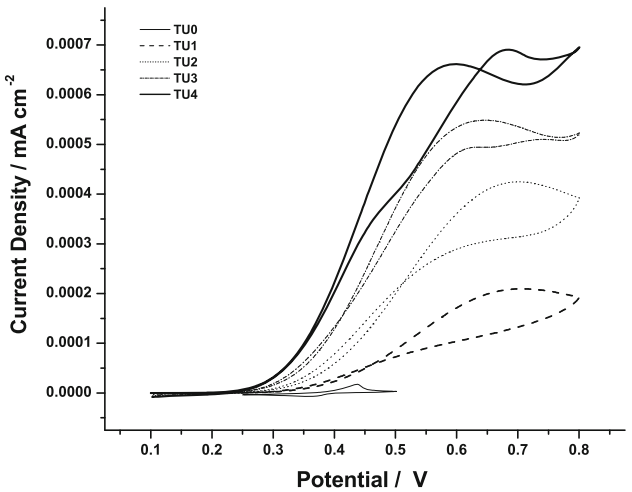

Fig. 7 Cyclic voltammetry of individual Ag^+ ion baths with compositions TU0–TU4 (Table 1)

of scan rate ($v^{1/2}$) is presented in Fig. 5. The behaviour suggests that the deposition process in the present bath composition is quasi-reversible. The non-linear dependence of I_{pc} on $v^{1/2}$ rules out the possibility of diffusion controlled deposition mechanism.

The CV curves of these ternary baths do not reveal any information about the species responsible for the change in current and broadening of the reduction peaks. Deciphering such behavior in a complex ternary bath is a daunting task. Instead, analysis of individual bath for metals with similar contents may help. In view of this, separate baths with only Sn, Ag and Cu salts were prepared while keeping the concentrations of all the other constituents identical. The CV curves of the bath containing only Sn, Ag and Cu are presented in Figs. 6, 7 and 8 respectively.

The CV curves of Sn (Fig. 6) bath show that there is a small shift in reduction potential after TU is added, which does not change anymore with increasing TU content. Similarly, the peak current is seen reducing after TU addition which does not change appreciably with subsequent TU addition. The CV curves for the baths containing only Ag^+ and Cu^{2+} ions are presented in Figs. 7 and 8 respectively. These curves (Figs. 7, 8) present a much different nature compared to the ternary baths. Firstly, the current range is about an order lower than that of Sn or the ternary baths, which may be due to equally smaller Ag and Cu ion content. Secondly, the reduction potentials are in the different range and there is a hint of an additional reduction peak that becomes prominent at higher TU content. The Ag and Cu species form various complexes with TU and its by-products which may be reducing

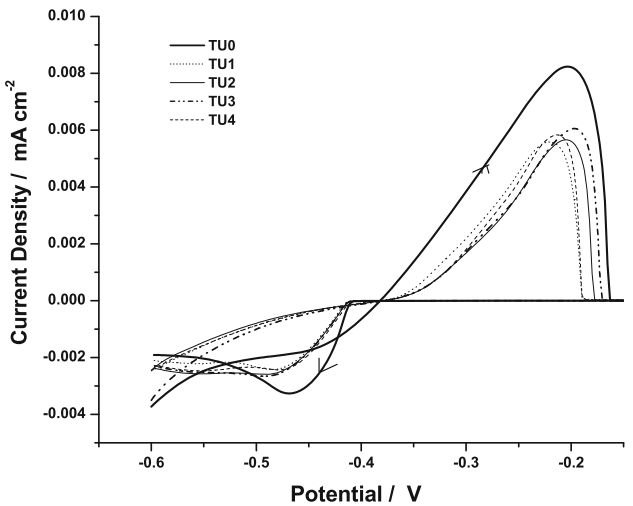

Fig. 6 Cyclic voltammetry of individual Sn^{2+} ion baths with compositions TU0–TU4 (Table 1)

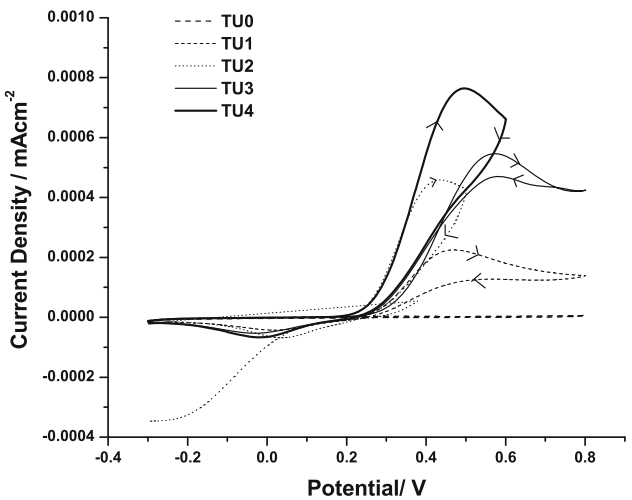

Fig. 8 Cyclic voltammetry of individual Cu^{2+} ion baths with compositions TU0–TU4 (Table 1)

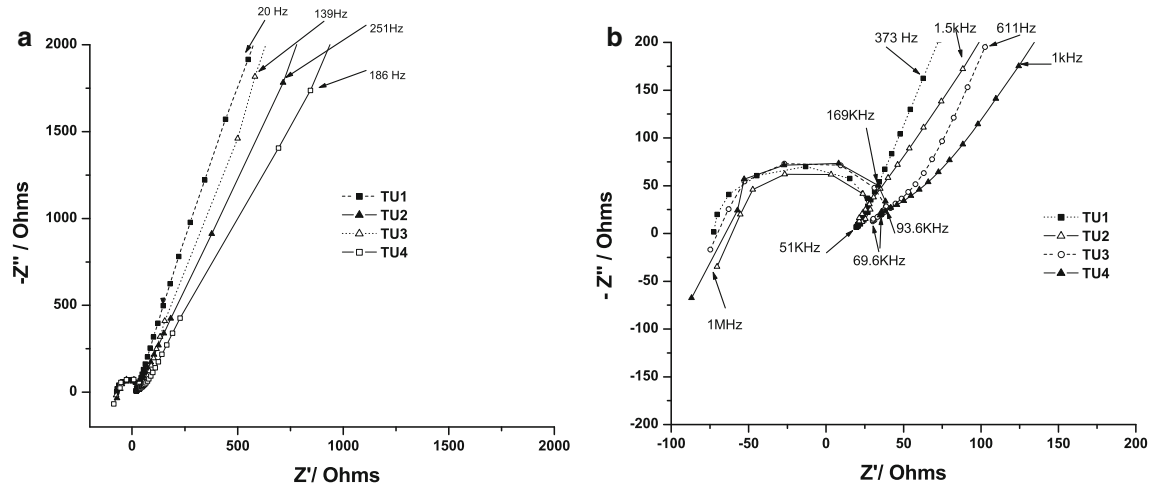

Fig. 9 Nyquist plots at 1 MHz to 1 mHz range for ternary Sn–Ag–Cu baths with compositions TU1–TU4 (Table 1) in **a** entire frequency range and **b** high frequency range

in close range of voltages, causing broadening of reduction peaks with increasing TU content.

3.3 Impedance analyses

In order to gain further insight into the microscopic processes and reactions taking place at the cathode, impedance analyses of all the ternary as well as individual baths were carried out in the frequency range of 1 MHz to 1 mHz and the corresponding Nyquist plots at different potentials were recorded. These potentials were chosen in a wide range from −0.56 to 0.06 V across the cyclic voltammetric sweep. On the whole, the nature of all the Nyquist plots was found to be identical. Figure 9 presents representative Nyquist plots for the ternary baths with varying TU concentrations, recorded at an intermediate potential of 0.06 V. A magnified view of the high frequency part of the spectra is presented separately in the figure. The curves show inductive behaviour at highest frequency, next a small high frequency capacitive loop up to a frequency range of about 100–200 kHz, which is followed by an apparently linear dependence up to about 100 Hz. Some negative differential capacitance is also seen at the intermediate frequencies. It was found that the spectra at further lower frequencies are erratic, and have been omitted. The difference between each spectrum is apparently small, but definite. It is seen that the diameter of the HF loops for TU1 and TU2 are close and smaller, while the same for TU3 and TU4 are slightly bigger and close to each other. On the other hand, the slope of low frequency straight line is found reducing with increasing TU concentration. It may be noted that χ^2 values for all the impedance analysis data presented here were found to be of the order of 10^{-2} to 10^{-3}, which attests for adequate reliability.

We attempted simulation of different equivalent circuits that could help understand the impedance spectra. Prima Facie, the nature of the Nyquist plots suggest that the RC and RL parallel combinations could help in explaining the high frequency capacitive loop and the straight line response at low frequencies, may be explained using Warburg resistance. However, attempts of including Warburg resistance failed, as the angle of the low frequency curve is much different from the expected 45°. Instead, a parallel combination of constant phase element (CPE) and resistor came close to the observed low frequency feature of the Nyquist plots. The circuit that produced closer results comprised of a parallel/series combination of resistors with inductor, capacitors and a CPE. For example, Fig. 10 presents typical simulated curves for circuits with Warburg resistance and CPE, superimposed on the experimentally observed plot for TU4. Deviation from Warburg resistance containing equivalent circuit and close match with the CPE containing equivalent circuit can be easily observed. Similar simulations were done for each of the TU curves shown in Fig. 9 to ascertain the range of values for each of the circuit elements.

The most striking feature of the plots in Fig. 9 is the consistent occurrence of negative real resistance at intermediate frequency, irrespective of TU content. Such behaviour is either due to the potential dependent adsorption of an inhibitor, deposition of catalyst, electrostatic effect at low ionic strength or a case when available electrode surface decreases with increasing polarization [11]. The negative real impedance has been regularly attributed to the presence of an inhibiting film on the cathode surface [15–17]. In this particular case, the negative resistance may be due to the adsorption of an insulating film that decreases the available surface area. This premise is supported by the observation of

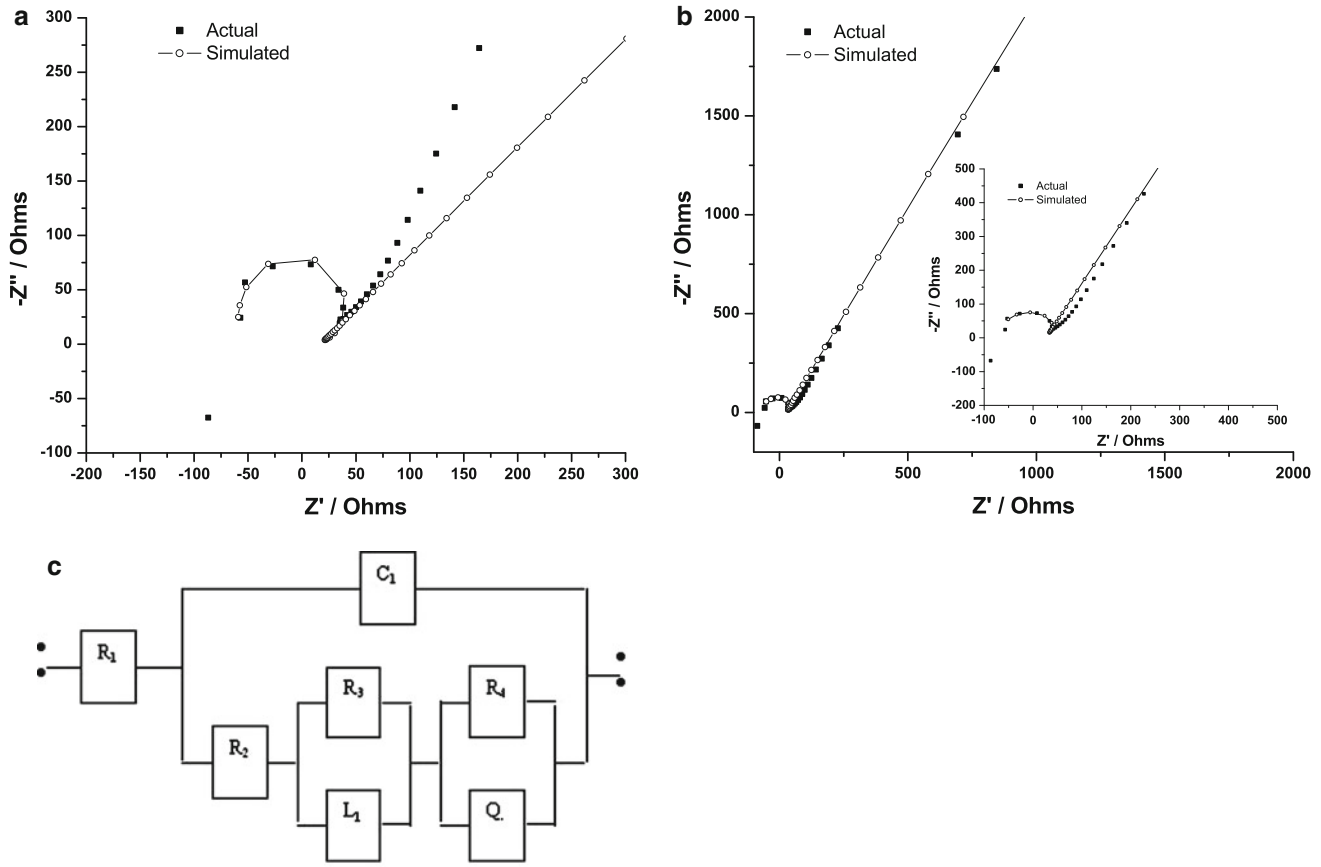

Fig. 10 Nyquist plots up to 100 Hz for ternary Sn–Ag–Cu baths with TU4 composition (Table 1), shown along with simulated plots considering **a** Warburg impedance and **b** CPE. The *inset* highlights matching of the simulated CPE curve in the high frequency range, and **c** the CPE based equivalent circuit with RCLQ components

reduced peak currents in the corresponding CV plots. In any case, the occurrence of negative real resistance seems to be independent of TU concentration in the given range. Another interesting feature of these Nyquist plots is the third quadrant inductive behavior at very high frequency. Such inductive behavior indicates instantaneous nucleation of the depositing species. The saturation nuclei density is related to the inductance by the relation $L \cong (N_s)^{1/2}$, where N_s is the saturation nuclei density [18]. Nucleation of depositing species involves extremely small time constants and is only expected to be observed at very high frequencies. In the present case, the Nyquist plots in Fig. 9 suggest increase in this inductance (1 MHz range) with increasing TU content, which is accompanied with higher nucleation density leading to refined microstructure of the films as seen evidently in Fig. 1.

The high frequency capacitive loop can be correlated to the double layer capacitance at the cathode surface and a parallel resistance, known as R_{ct} or the charge transfer resistance, across the double layer. From the equivalent circuit used to explain the nature of Nyquist plots, the charge transfer resistance can be correlated to the addition of the resistances R_2 and R_3 [19]. It is seen that the R_{ct} for the present system is in the range of 160–199 Ω, while the double layer capacitance, viz. C_1 in the equivalent circuit, is in the range of 0.1–0.5 μF cm^{-2}. The R_{ct} values do not show any dependence on TU concentration, which is expected in the given range of its variation [20]. Generally, the double layer capacitance is expected to be in the range of 10–40 μF cm^{-2} [21]. Such lower value of double layer capacitance points towards un-availability of full electrode surface during deposition and confirms presence of an insulating film on the surface. Obviously, the metal ions must be involved in removal of these adsorbed species, which shows up in the form of negative differential capacitance at the beginning of the low frequency CPE loop. It is known that such inductive behaviour indicates relaxation [22].

The impedance spectra for all the TU concentrations show a low frequency behaviour that fits well with the CPE model, with '*n*' in the range of 0.65 to 0.8, Q varying from 0.05 to 0.1S.s^n and its parallel resistance varying from 85 to 100 kΩ. There is no clear trend in these values at different TU concentrations. Such a low frequency response points towards adsorption of a poor quality, non-uniform, insulating film or an exponentially decreasing conductivity of

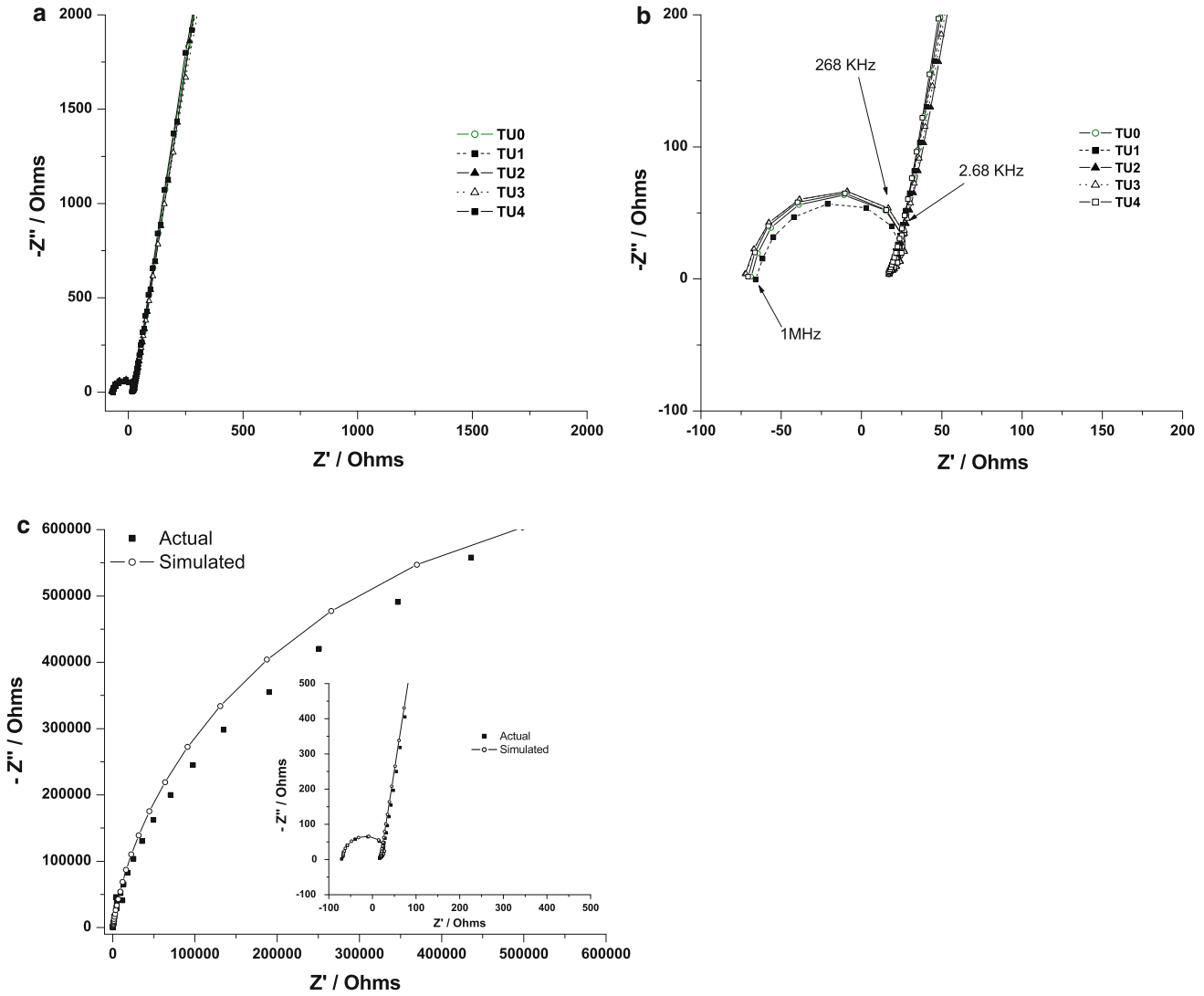

Fig. 11 Nyquist plots at 1 MHz to 1 mHz range for individual Sn^{2+} ion baths with compositions TU0–TU4 (Table 1). **a** Entire frequency range, **b** high frequency range, and **c** the TU4 composition along with the simulated curve with CPE element in entire frequency range and high frequency range (*inset*)

this film, mostly stemming from non-stoichiometry [23]. In fact, the un-correlated and un-decipherable data at frequencies below 75–100 Hz may have been caused by this poor quality insulating film present on the surface.

In order to understand the nature of ternary Nyquist plots, similar impedance analyses of the individual Sn, Ag and Cu ion baths was carried out. Figure 11 presents the Nyquist plots for the Sn baths. These curves are strikingly similar to the ternary baths with similar features, such as, a small high frequency capacitive loop, followed by an inductive loop, and an apparently linear curve until about 10 Hz. Thereafter, these Nyquist plots also produce uninterpretable data.

Similar looking Nyquist plots have been recorded for the individual Ag and Cu baths which are presented in Figs. 12 and 13 respectively. A high frequency capacitive loop followed by an inductive loop is a common feature in all the Nyquist plots. For all the individual baths, the series resistance R_s (about $-70\ \Omega$) and the charge transfer resistance R_{CT} (170–200 Ω), are in the same range as for the ternary bath. However, the double layer capacitance shows an increase of about one order magnitude (20–25 nF) and there is a difference in the low frequency CPE loops for all individual baths compared to the ternary bath.

It is seen that all the individual ion baths have the '*n*' value restored to 0.9 or above, and the 'Q' of the CPE increased by about two orders of magnitude than that for the ternary baths. These values indicate capacitive behaviour at low frequencies, possibly indicating an improved quality of the insulating film. The low frequency CPE loops for the Sn

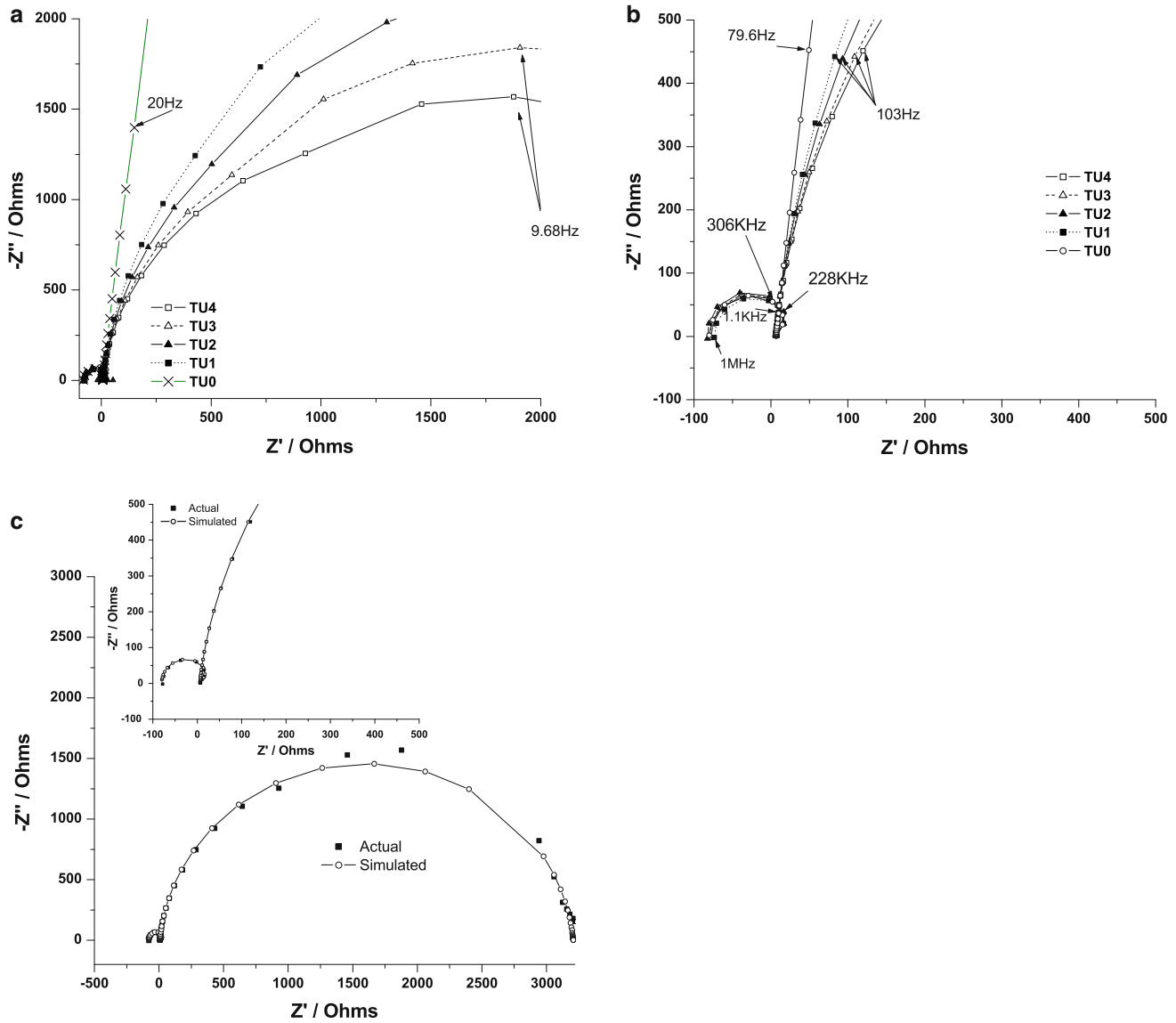

Fig. 12 Nyquist plots at 1 MHz to 1 mHz range for individual Ag^{+} ion baths with compositions TU0–TU4 (Table 1). **a** Entire frequency range, **b** high frequency range, and **c** the TU4 composition along with the simulated curve with CPE element in entire frequency range and high frequency range (*inset*)

baths are relatively large and almost independent of the changing TU concentration. This indicates very weak influence of TU on Sn. This confirms our earlier observation that Sn is not held in chelation by TU, while TU does chelate with Ag and Cu [6]. Contrary to the Sn baths, the low frequency CPE loops of the Ag and Cu baths show reduction in the diameter with increasing TU content. Thus, the resistance parallel to CPE (R_4) reduces from ~ 7 kΩ to 3 kΩ with increasing TU concentration. It is reported that smaller low frequency capacitive loop indicates improved deposition quality [22]. Although there is no clear trend, there is a hint of similar reduction in the size of CPE loop for the ternary baths in Fig. 9, while improved deposition quality is seen in the SEM micrographs in Fig. 1.

The close similarity of high frequency loop and related features until the low frequency feature begins for all the ternary and individual baths indicate that the origin of these features lie in the additives other than the TU, the metal ions or their chelates. We investigated this aspect by recording the Nyquist plots for baths containing Sn ions in MSA and distilled water, as well as for a bath having only MSA and distilled water. Interestingly, it was found that both the baths show almost similar HF features comprising of a high frequency capacitive loop, followed by an inductive loop at intermediate frequency. The low frequency feature for the bath having Sn in MSA and distilled water is again similar, but the same for the MSA with distilled water bath was different. The negative series

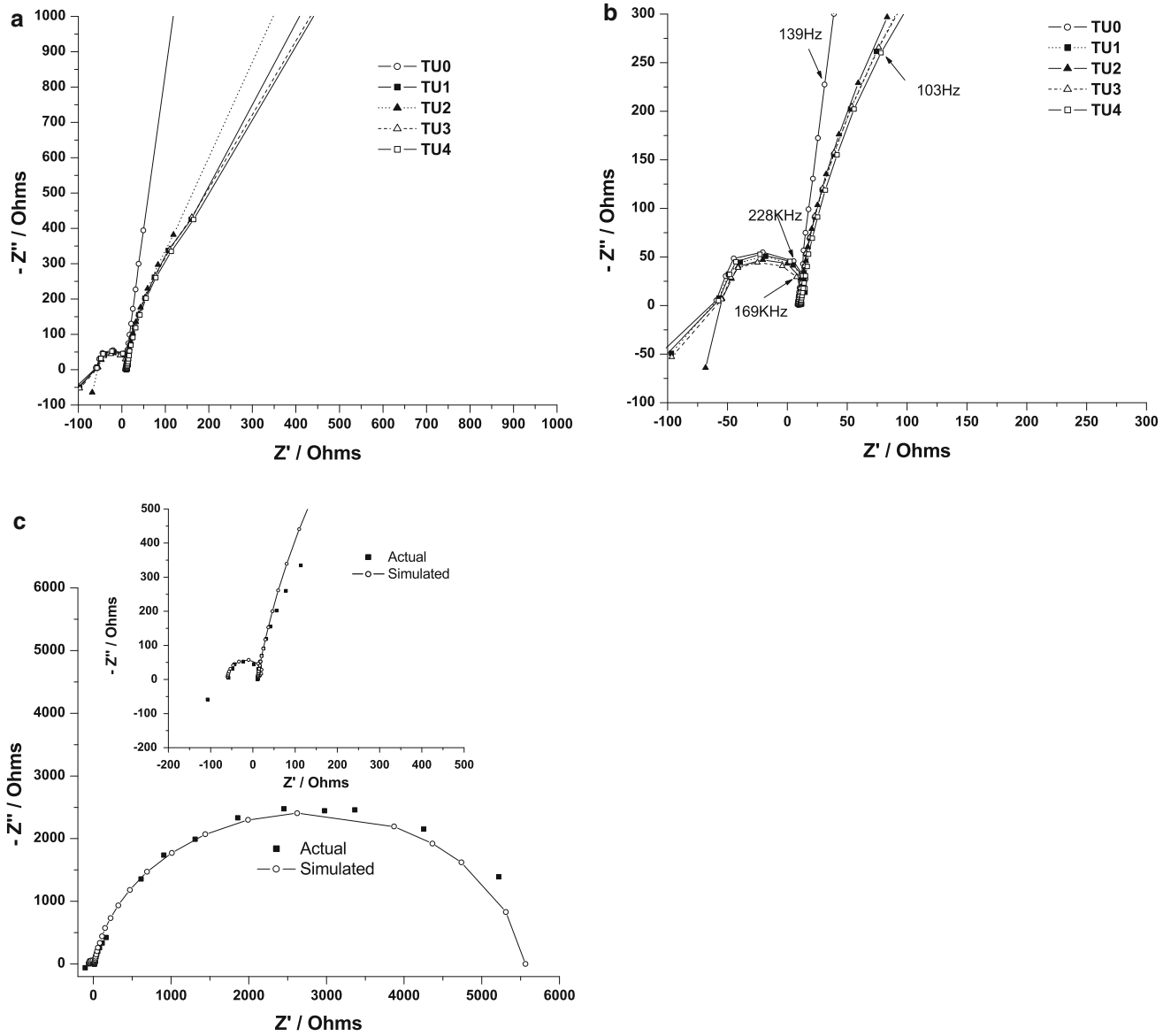

Fig. 13 Nyquist plots at 1 MHz to 1 mHz range for individual Cu^{2+} ion baths with compositions TU0–TU4 (Table 1). **a** Entire frequency range, **b** high frequency range, and **c** The TU4 composition along with the simulated curve with CPE element in entire frequency range and high frequency range (*inset*)

resistance value for both the baths is found to be in the same range of about −70 Ω. This similarity between the ternary baths and the almost fully stripped baths clearly indicates that the adsorbed impeding species is contributed either by MSA or water. It is known that adsorbed Hydrogen does impede the depositions [22] and protonic transfer between MSA and water is also reported [24]. While removal of this film during deposition causes the negative differential capacitance, the low frequency CPE is probably contributed by the loosely adsorbed TU and other additives on to the growing film. This adsorption forces new nucleating sites, resulting in finer grain structures.

4 Conclusions

A MSA based ternary electrolytic bath for co-deposition of Sn–Ag–Cu solder films has been developed in-house. Detailed electrochemical investigations have been conducted in order to understand the microscopic processes taking place during deposition. Impedance analyses of baths containing different concentrations of TU, which functions as chelating agent for Ag and Cu ions, has been carried out. These studies helped in correlating the electrolytic system to an equivalent circuit and understand the contribution of TU in enhancing or inhibiting the

deposition process. In the present bath system, it is clear that TU or its oxidized form enter into chelation with Ag or Cu ions alone, while Sn may be only having some loose, hydrogen bonding like bonding with the additives. It is clear that these chelated ions deposit separately in a very close range of potentials. TU helps in refining the microstructure of the films, which is also confirmed from the impedance spectra. The bath produces close to eutectic composition for Sn–Ag–Cu films, with somewhat higher Cu content. The nature of impedance spectra evidently indicates adsorption of an insulating film on the cathode surface, contributed by MSA or water. This film loses its covered area to metal ions through competitive deposition, which shows-up in the form of mid frequency negative differential capacitance. The growing metal film is covered by a loosely adhered insulating film of additives which cause newer nucleation, leading to refined microstructure with increasing TU content. In general, the present investigation has improved our understanding of the microscopic processes during co-deposition of the ternary Sn–Ag–Cu films. More precise understanding of the bath demands chemical or spectroscopic analysis of the bath and similar studies at different pH values.

Acknowledgments This work was fully supported by Centre for Materials for Electronics Technology (C-MET) through the generous grants from the Department of Information Technology, Government of India. The authors are thankful to Dr. D. P. Amalnerkar, Executive Director, C-MET, for his unflinching support and guidance.

References

1. Laalonde A, Emelander D, Jeannette J, Larson C, Rietz W, Swenson D, Henderson DW (2004) J Electron Mater 33:1545
2. Anderson IE, Cook BA, Harringa J, Terpstra RL (2002) J Electron Mater 31:1166
3. Zhang J, An M, Chang L, Liu G (2008) Electrochim Acta 53:2637
4. Pang JHL, Xiong BS (2005) IEEE Trans Comp Packag Technol 28:830
5. Ou S, Tu KN (2005) Proc IEEE ECTC, p 1445
6. Joseph S, Phatak G (2008) Surf Coat Technol 202:3023
7. Nawafune H, Shiba K, Akamatsu K, Mizumoto S, Uchida E, Obata K (2002) J Jpn Inst Elect Packag 5(2):146
8. Gherrou A, Kerdjoudj H, Molinari R, Drioli E (2001) Sep Purif Technol 22–23:571
9. Ozga P (2006) Arch Metall Mater 51:413
10. Ashiru OA, Farr JPG (1995) J Electrochem Soc 142:3729
11. Survila A, Mockus Z (1999) Electrochim Acta 44:1707
12. Lacconi GI, Macagno VA (1994) Electrochim Acta 39:2605
13. Mouanga M, Ricq L, Bercot P (2008) J Appl Electrochem 38:231
14. San Martin V, Sanllorente S, Palmero S (1998) Electrochim Acta 44:579
15. Epelboin I, Joussellin M, Wiart R (1979) J Electroanal Chem 101:281
16. Goldbach S, de Kermade R, Lapicque F (2000) J Appl Electrochem 30:277
17. Gudic S, Radosevic J, Kliskic M (2002) Electrochim Acta 47:3009
18. Bozzini B, Mele C, Sgura I (2004) J Appl Electrochem 34:277
19. Lee K-K, Kim K-B (2001) Corros Sci 43:561
20. Kang MS, Kim S-K, Kim K, Kim JJ (2008) Thin Solid Films 516:3761
21. Loveday D, Peterson P, Rodgers B (2004) JCT CoatingsTech 1:88
22. Holm M, O'Keefe TJ (2000) J Appl Electrochem 30:1125
23. Frateur I (2008) ECS Trans 13:115
24. Wang L (2007) J Phys Chem 111:3642